ADVANCED ENERGY & SUSTAINABILITY RESEARCH
Open Access
www.advenergysustres.com

Progress in Metafibers for Sustainable Radiative Cooling and Prospects of Achieving Thermally Drawn Metafibers

*Miao Qi, Tingting Wu, Zhe Wang, Zhixun Wang, Bing He, Haozhe Zhang, Yanting Liu, Jiwu Xin, Tianzhu Zhou, Xuhui Zhou, and Lei Wei**

The growing awareness of the energy crisis and global warming has inspired researchers to pursue alternative cooling strategies. Radiative cooling is an environmentally friendly approach that dissipates excessive heat through the atmospheric long-wave infrared transmission window (8–13 μm) to the cold universe. Metamaterials with unique photonic structures are applicable to radiative cooling and have been extensively studied. Incorporating meta-elements to the fiber level of the fabric to construct metafibers is expected to achieve personal thermal management through radiative cooling. Compared with the conventional fiber manufacturing methods, the thermal drawing technique can mass-produce multimaterial and multifunctional fibers with well-defined structures. These in-fiber micro- and nanostructures of light wavelength scale possess great potentials in radiative cooling applications, providing bright prospects for a new generation of metafiber-based smart fabrics. Herein, the fundamental principles of radiative cooling and the metamaterials being used for radiative cooling are summarized. The textiles used for personal cooling and their preparation methods are also introduced. Finally, the article focuses on the preparation of micro- and nanostructures by the thermal drawing technique, which provides a potential solution for the large-scale manufacture of metafibers for sustainable radiative cooling.

1. Introduction

The building sector has consumed over 30% of the world's total annual energy supply. A considerable portion of the building energy consumption is the space cooling for human thermal comfort.[1] With the growing awareness of the energy crisis and global warming, many ideas have been put forward to pursue alternative cooling strategies to minimize the energy requirements.[2] It has been reported that increasing the desirable preset cooling temperature by 2 °C can save 20% of the energy consumed for temperature regulation in indoor space.[3] Therefore, instead of cooling the entire building to a relatively low temperature, developing personal thermal management techniques that provide localized thermal comfort around the human body will effectively alleviate the energy consumption.[4,5]

Radiative cooling is a ubiquitous process that exploits the balance of radiative heat flow to dissipate excessive heat through the atmospheric long-wave infrared transmission window (8–13 μm) to the cold universe.[6,7] Notably, the human body strongly emits thermal radiation in the wavelength range of 7–14 μm, accounting for more than 50% of the total body heat dissipation.[8] Thus, it is a promising approach towards personal thermal management through this energy-free radiative cooling process. Choi et al. achieved radiative cooling by native silk with nanostructures.[9–11] However, most of the traditional fabrics, like cotton, wool, and polyester, usually lack the capability of infrared radiation control. Fortunately, with the development of radiative cooling technology, in recent years, many infrared-transparent textiles have been proposed to allow the thermal radiation from the human skin to reach the ambiance directly.[12]

In addition, to realize daytime radiative cooling under direct sunlight, it requires not only a high emissivity within the infrared atmospheric window, but also a near-zero absorptivity in the solar spectrum.[13,14] Thanks to the advent of metamaterials, diurnal subambient cooling under direct sunlight has been achieved.[15–24] Metamaterials are engineered materials with unique photonic structures that do not exist in nature and can be used to manipulate electromagnetic waves.[24–31] Since their optical properties can be selectively designed by adjusting structural parameters, metamaterial-based radiative cooling has attracted extensive research attention.[32] More intriguingly, Zhang et al. fabricated a metatextile with dynamic adaptive infrared optical properties, which incorporated the meta-element to the fiber level of the fabric and achieved synergistically enhance infrared gating effects.[33]

M. Qi, T. Wu, Z. Wang, Z. Wang, B. He, H. Zhang, Y. Liu, J. Xin, T. Zhou, X. Zhou, L. Wei
School of Electrical and Electronic Engineering
Nanyang Technological University
50 Nanyang Avenue, Singapore 639798, Singapore
E-mail: wei.lei@ntu.edu.sg

The ORCID identification number(s) for the author(s) of this article can be found under https://doi.org/10.1002/aesr.202100168.

DOI: 10.1002/aesr.202100168

Noticing that fibers are the cornerstones of textiles, developing metafibers is crucial to the advance in metatextiles.[6] Therefore, approaches such as melt spinning, wet spinning, dry spinning, electrospinning, and thermal drawing are investigated by researchers for fiber manufacturing.[34] Among all these methods, the preform-to-fiber thermal drawing approach developed to fabricate kilometer-long cladding-core structure glass fiber offers the capability to embed multimaterials and multifunctions into one fiber.[35,36] In addition, in recent years, many approaches such as thermal treatment,[37–45] cold-drawing,[46] direct imprinting,[47–51] etc., have been adopted for the fiber postprocessing to construct uniform micro- and nanostructures in thermally drawn fibers. This provides a novel solution for the mass production of metafibers, which is promising for personal thermal management.[52]

This review aims to propose potential research prospects for the manufacture of fiber-based metamaterials and their applications in radiative cooling. First, we briefly introduce the fundamental principles, materials, and structures of radiative cooling. Then, the metamaterials currently being used for radiative cooling are summarized. Majorities are films of inorganic photonic structures. Subsequently, we present polymer-based textiles for personal cooling, including the fabrication methods of these fibers. Finally, we focus on the development of the thermal drawing technique and give an intriguing solution for manufacturing fiber-based metamaterials for the future radiative cooling.

2. Fundamental Principles for Radiative Cooling

Cooling is essential in human life. However, conventional cooling systems, such as fans, air conditioners, or thermoelectric, consume considerable energy and are accompanied by greenhouse gas emissions.[53] With the development of human society, there is an urgent need for alternative cooling technologies which are energy free and environmentally friendly. Radiative cooling is a passive and energy-free way to radiate heat into the cold universe through the atmospheric window. All materials absorb and emit electromagnetic waves, and materials with higher temperatures emit stronger. Thus, heat flows from hot objects to cold bodies through these energy-carrying electromagnetic waves. Considering that the surface temperature of the Earth is near 300 K, while the universe has a typical temperature of 3 K, the large temperature difference can be exploited to cool the planet.[22] The emission spectrum of a blackbody at 300 K is shown in **Figure 1** (black line), which matches well with the transmittance spectrum of the atmospheric window (8–13 μm) (blue area). Thus, objects on the surface of the Earth can be cooled by emitting thermal infrared radiation to outer space through the atmosphere, i.e., radiative cooling.[13]

The Earth absorbs short-wavelength solar irradiation and emits infrared radiation to maintain energy balance. Given P_{solar} the solar irradiation power, P_{atm} the absorbed atmospheric radiation power, P_{rad} the thermal radiation power from the surface, and $P_{\text{nonradiative}}$ the nonradiative heat transfer like conduction and convection, the net cooling power P_{net} of a radiator according to energy balance theory can be expressed as

$$P_{\text{net}} = P_{\text{rad}} - P_{\text{atm}} - P_{\text{solar}} - P_{\text{non-radiative}} \tag{1}$$

Atmospheric radiation is mainly induced by H_2O, CO_2, and O_3, while the absorptivity/emissivity of N_2 and O_2 is relatively low. It affects solar irradiation (0.3–3 μm) and thermal infrared radiation (3–50 μm). P_{atm} is mainly contributed by the wavelengths outside the atmospheric window, at the absolute air temperature T_{amb}, P_{atm} can be expressed as

$$P_{\text{atm}}(T_{\text{amb}}) = A \int \cos\theta d\Omega \int_0^{\infty} I_{\text{bb}}(\lambda, T_{\text{amb}}) e_{\text{atm}}(\lambda, \theta) d\lambda \tag{2}$$

where A is the area of the radiating material, $\int d\Omega = 2\pi \int_0^{\pi/2} \sin\theta d\theta$ is the angular integral over a hemisphere, $I_{\text{bb}}(\lambda, T_{\text{amb}}) = (2hc^2/\lambda^5)(e^{hc/\lambda k_B T_{\text{amb}}} - 1)^{-1}$ is the blackbody spectral radiance at temperature T_{amb}, h is the Planck's constant, c is the speed of light in vacuum, k_B is the Boltzmann constant, λ is the wavelength, and $e_{\text{atm}}(\lambda, \theta) = 1 - \text{t}(\lambda)^{1/cos\theta}$ is the spectral and angular emissivity with $t(\lambda)$ being the atmospheric transmissivity in the zenith direction. The absorbed solar power P_{solar} by the radiator can be expressed as

$$P_{\text{solar}} = A \int_0^{\infty} I_{\text{AM1.5}}(\lambda) e(\lambda, \theta_{\text{sun}}) d\lambda \tag{3}$$

where $I_{\text{AM1.5}}(\lambda)$ is the solar illumination intensity, θ_{sun} is the angle between the incident solar irradiation and the surface. The power loss caused by nonradiative heat transfer can be expressed as

$$P_{\text{nonradiative}}(T, T_{\text{amb}}) = A h_{\text{tot}}(T_{\text{amb}} - T) \tag{4}$$

where h_{tot} is the nonradiative heat coefficient. The total radiated power from a surface with a temperature of T_s can be expressed as

$$P_{\text{rad}}(T_s) = A \int \cos\theta d\Omega \int_0^{\infty} I_{\text{bb}}(\lambda, T_s) e(\lambda, \theta) d\lambda \tag{5}$$

where $e(\lambda, \theta)$ is the emissivity of the surface. Within the temperature range of interest, it can be assumed that $e(\lambda, \theta)$ is independent of temperature and only has angular and spectral correlation. In radiative cooling, the emissivity in the zenith direction of the atmospheric window is mainly considered. To optimize the radiative cooling power, P_{rad} should be maximized, and P_{atm}, P_{solar}, and $P_{\text{nonradiative}}$ should be minimized. Therefore, in short, the most superior radiative cooling material should possess a low emissivity (high reflectivity) in the solar spectrum (0.3–3 μm) and a high thermal emissivity in the atmospheric window (8–13 μm) (Figure 1).

3. Metamaterial-Based Radiative Cooling

Based on the principles for radiative cooling, the radiation characteristic of a radiator is the key parameter of effective cooling. The advent of metamaterials has rendered radiative cooling feasibility in real life. Metamaterials are artificial structures with controllable photonic features designed to achieve broadband emission in the atmospheric window. Generally, three kinds of metamaterials are

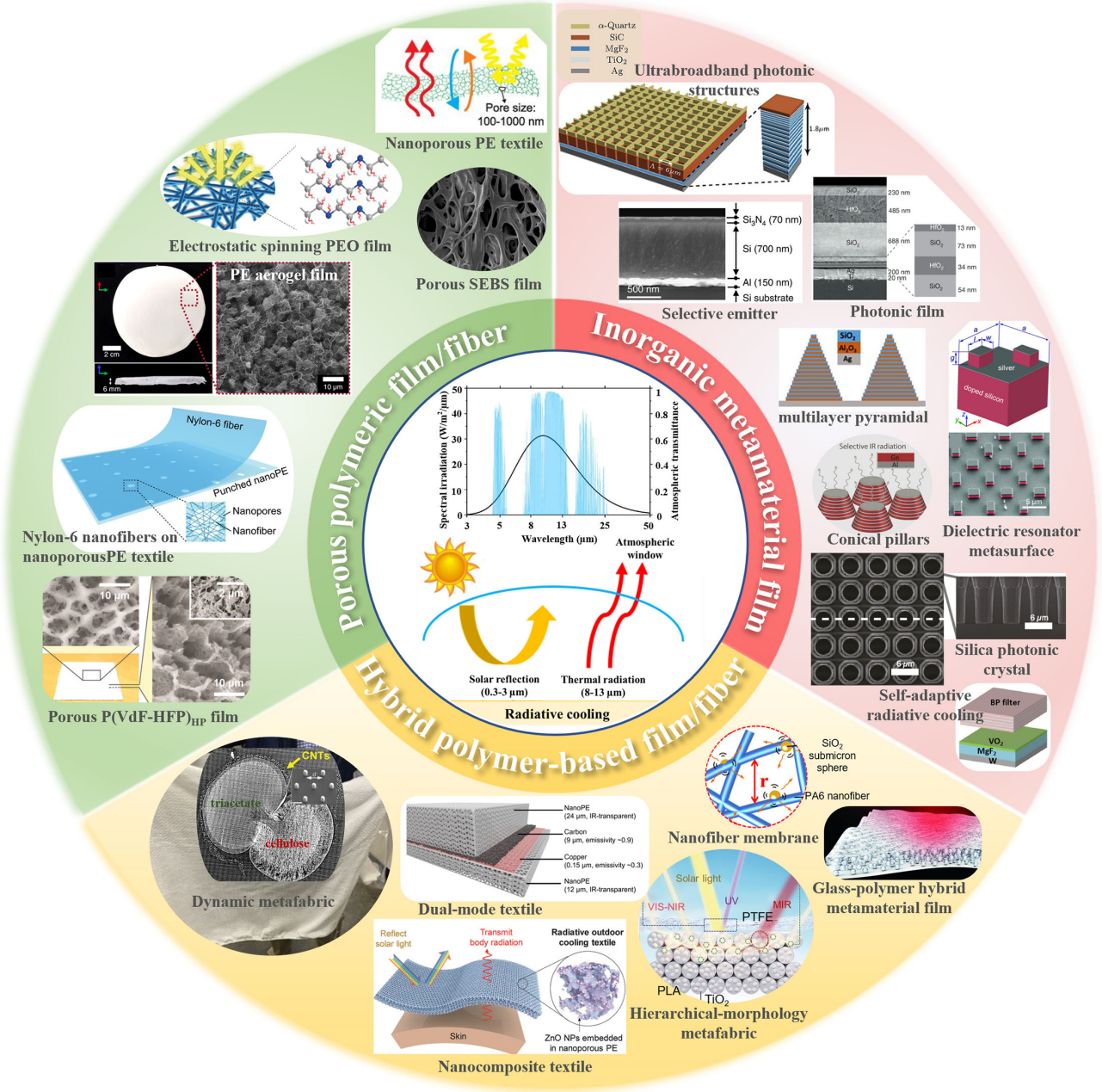

Figure 1. Fundamental principles and materials for radiative cooling. Reproduced with permission.[8] Copyright 2016, American Association for the Advancement of Science (AAAS). Reproduced with permission.[97] Copyright 2021, Springer Nature. Reproduced with permission.[98] Copyright 2020, AAAS. Reproduced with permission.[99] Copyright 2019, AAAS. Reproduced with permission.[100] Copyright 2017, American Chemical Society. Reproduced with permission.[101] Copyright 2018, AAAS. Reproduced with permission.[17] Copyright 2013, American Chemical Society. Reproduced with permission.[22] Copyright 2016, Springer Nature. Reproduced with permission.[21] Copyright 2014, Springer Nature. Reproduced with permission.[24] Copyright 2018, Elsevier. Reproduced with permission.[27] Copyright 2017, Wiley-VCH GmbH. Reproduced with permission.[25] Copyright 2015, Wiley-VCH GmbH. Reproduced with permission.[20] Copyright 2015, United States National Academy of Sciences. Reproduced with permission.[23] Copyright 2018, The Optical Society. Reproduced with permission.[102] Copyright 2017, AAAS. Reproduced with permission.[66] Copyright 2018, Wiley-VCH GmbH. Reproduced with permission.[103] Copyright 2019, American Chemical Society. Reproduced with permission.[69] Copyright 2021, AAAS. Reproduced with permission.[26] Copyright 2017, AAAS. Reproduced with permission.[33] Copyright 2019, AAAS.

proposed for radiative cooling, i.e., nanoantenna-based, multilayer-based, and microparticle-based radiators.

Nanoantenna-based radiators possess a high degree of freedom for tailoring the spectral selectivity by designing the patterned surface. Rephaeli et al. demonstrated the possibility of daytime radiative cooling by using an ultrabroadband patterned surface.[17] As shown in **Figure 2**a, the design consists of two layers. The top layer is a 2D periodic photonic design

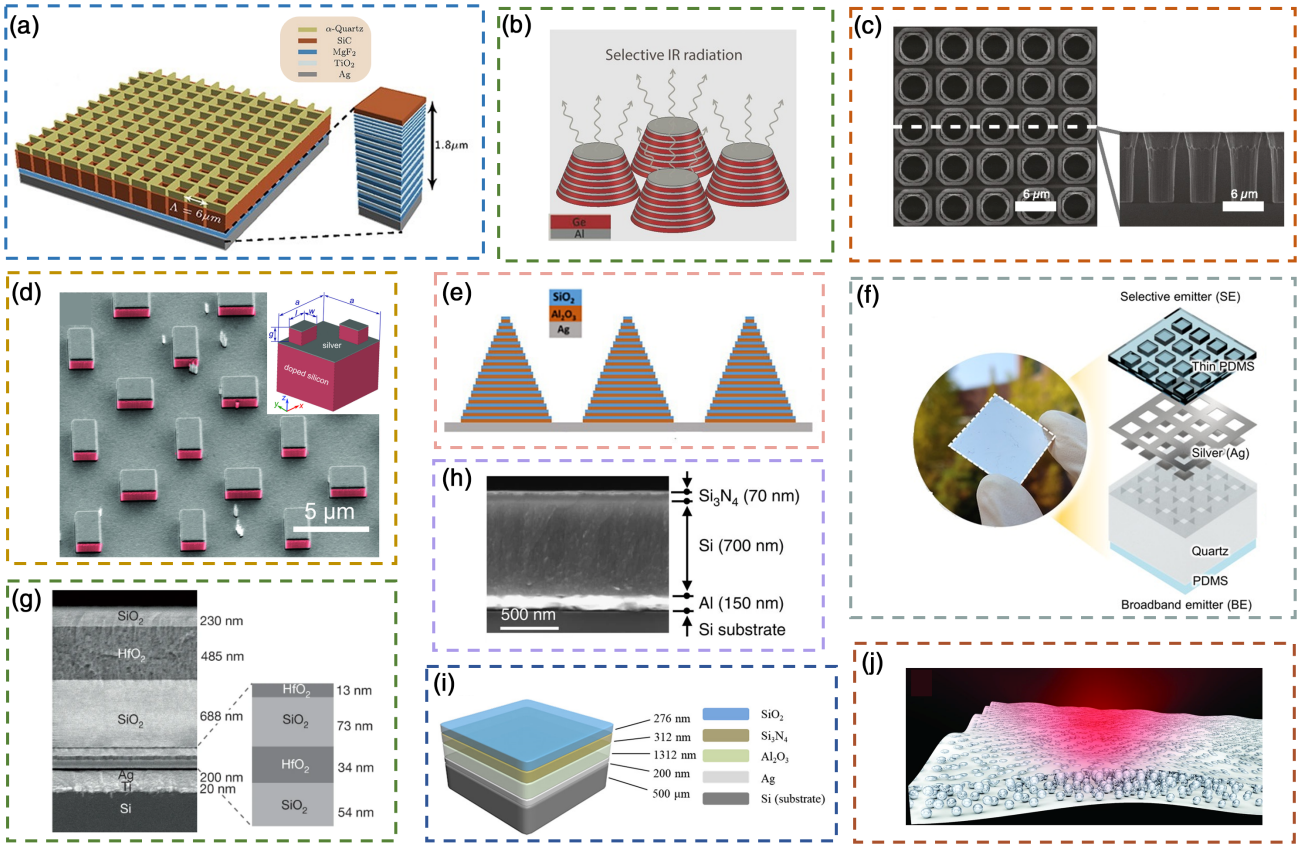

Figure 2. Various metamaterials used for radiative cooling. a) Diagram of ultrabroadband metal-dielectric photonic structures. Reproduced with permission.[17] Copyright 2013, American Chemical Society. b) Diagram of conical-shaped metamaterial emitter. Reproduced with permission.[25] Copyright 2015, Wiley-VCH GmbH. c) SEM image of visibly transparent silica photonic crystal. Reproduced with permission.[20] Copyright 2015, United States National Academy of Sciences. d) SEM image of dielectric resonator metasurface. Reproduced with permission.[27] Copyright 2017, Wiley-VCH GmbH. e) Diagram of a pyramidal nanostructure. Reproduced with permission.[24] Copyright 2018, Elsevier. f) Diagram of Janus emitter. Reproduced with permission.[29] Copyright 2020, AAAS. g) SEM image of HfO_2-SiO_2 photonic film. Reproduced with permission.[21] Copyright 2014, Springer Nature. h) SEM image of the radiative emitter. Reproduced with permission.[22] Copyright 2016, Springer Nature. i) Diagram of the inorganic radiative cooler structure. Reproduced with permission.[54] Copyright 2020, American Chemical Society. j) Diagram of the scalable-manufactured glass-polymer hybrid metamaterial. Reproduced with permission.[26] Copyright 2017, AAAS.

of quartz and SiC. These two materials are transparent for solar radiation and possess resonances at 9.3 and 12.5 μm to cover the entire atmospheric window. In addition, the surface phonon–polariton modes can further enhance the broad-angle emission. The bottom layer is a reflector to minimize the solar irradiation and consists of three sets of five alternating bilayers of TiO_2 and MgF_2, and these sets have varying periods to generate three overlapping photonic bandgaps. The simulation result reveals that P_{net} exceeds 100 W m^{-2} at T_{amb}. Hossain et al. designed a conical-shaped metamaterial emitter composed of alternating circular layers of Al and Ge on a Si substrate (Figure 2b).[25] Through parameters optimization, the emitter can achieve high emissivity in the atmospheric window while maintaining the solar transparency and a practical P_{net} of 116.6 W m^{-2} is delivered. In addition to the abovementioned solar reflective metamaterials, in 2015, Zhu et al. demonstrated a visibly transparent thermal blackbody (Figure 2c).[20] The blackbody is a silica photonic crystal fabricated by etching 10 μm depth air holes into a silica wafer. Silica is selected as the primary constituent material due to its solar wavelength transparency and two main strong phonon–polariton resonances near 10 and 20 μm. The phonon–polariton resonances correspond to large reflectivity and small emissivity, and this defect is modified by nano-/microstructures, such as pyramids (Figure 2e) and air holes (Figure 2c). When placed on a Si absorber, the silica photonic crystal can realize a temperature drop of 13 °C by radiative cooling. In 2017, Zou et al. fabricated a dielectric resonator metasurface, which is expected to be manufactured on a large scale.[27] As displayed in Figure 2d, the metasurface is composed of phosphorus-doped n-type Si and Ag. The doped-Si is selected to achieve the required emissivity at infrared frequencies, and Ag is necessary for enhancing solar reflection. Owing to the magnetic dipole resonance of the dielectric resonator metasurface, a temperature drop of 7.36 °C is realized in the daytime. Wu et al. numerically demonstrated a pyramidal nanostructure composed of alternating aluminum oxide and silica layers, which is a near-perfect absorber for radiative cooling (Figure 2e).[24] Although radiative cooling has been vigorously developed, cooling enclosed spaces

is still a challenge. Based on this, Heo et al. proposed a Janus emitter with a polymer-based selective emitter (SE) on the top and a broadband emitter (BE) on the bottom for automobile cooling under direct sunlight.[29] As shown in Figure 2f, the manufactured emitter consists of a 4 μm-thick polydimethylsiloxane (PDMS) layer, an Ag layer that reflects solar light and isolates the top and bottom sides, a micropatterned quartz layer, and a 10 μm-thick PDMS layer. The Ag–PDMS groove (SE) induces spoof surface plasmon polariton resonance to overcome the inherent emissivity loss of PDMS. The BE can absorb thermal input, while SE emits heat. The fabricated Janus emitter can reduce the temperature inside an enclosure by about 4 °C.

Multilayer-based radiators are 1D and consist of alternating thin dielectric layers with different dielectric materials and permittivities. The layer number and each layer thickness are the vital geometric parameters for spectral controlling and the corresponding real applications. For the recently proposed multilayer-based radiators,[21–23,54–60] silicon dioxide, silicon carbide, and silicon nitride are widely applied due to the weak extinction in the solar radiation spectrum and strong extinction peaks in the mid-infrared band. Metallic thin films, such as silver and aluminum films, are the best choice for reflective layers. Raman et al. experimentally reported an integrated thermal emitter including seven alternating layers of HfO_2 and SiO_2 (Figure 2g).[21] HfO_2 is a high-index material, while SiO_2 is a low-index layer. The thickness of the bottom four layers is less than 100 nm to optimize solar reflection, while the top three layers are much thicker to emit thermal radiation. The fabricated photonic radiator can achieve a P_{net} of 40.1 W m^{-2} with a temperature drop of 4.9 °C. Subsequently, the researchers improved the structure and performance of the photonic film by theoretical analysis and rational experimental design.[22] As shown in Figure 2h, the emitter is composed of Si_3N_4, amorphous Si, and Al layers on a Si wafer. The phonon–polariton excitation of Si_3N_4 induces emission in the atmospheric window, and the thickness is small enough to avoid unexpected radiative loss. This research combines photonic and thermal design to achieve an average temperature drop of 37 °C through a 24 h day–night cycle. A similar multilayer structure composed of SiO_2, Si_3N_4, and Al_2O_3 has also been developed to realize daytime radiative cooling (Figure 2i).[54]

Although numerous inorganic nanophotonic structures have been developed for effective radiative cooling in the laboratory, large-scale manufacturing is still a challenge due to the precision lithography and deposition required for their fabrication process. Moreover, the intrinsic fragility of inorganic materials limits the applications of these emitters. Fortunately, Zhai et al. proposed a ground-breaking approach for the scalable manufacturing of metamaterial thin film.[26] As depicted in Figure 2j, in the metamaterial, SiO_2 microspheres are randomly encapsulated in a polymethylpentene (TPX) polymer matrix. TPX is transparent to the solar spectrum, and SiO_2 microspheres with an optimized diameter possess a high infrared emissivity through phonon-enhanced Fröhlich resonances. Therefore, thermal emission in 8–13 μm atmospheric window is strongly enhanced, and the transparency to solar radiation is fully maintained. The glass–polymer hybrid metamaterial film with a thickness of 50 μm is fabricated in a roll-to-roll way. After being coated with a 200 nm-thick Ag film on its back, the metamaterial can provide an average P_{net} of >100 W m^{-2} over a successive 72 h test. This work has inspired some other studies on the application of metamaterials based on random particles in radiative cooling, which are easy to manufacture and usually possess flexibility obtained from polymers.[61–63]

4. Fibers for Human Body Cooling

Thermal comfort is of great significance to human life, and it directly influences personal health, mood, and work productivity.[1] In recent years, the energy consumption of space cooling in the global commercial and residential sectors has increased rapidly.[64] The localized "personal thermal management" concept using innovative textiles to cool the human body provides an effective alternative to this problem and avoids wasted excess power for cooling the entire building.[4,5] Thus, as the building blocks of textiles, a variety of fibers have been designed to achieve human cooling, and majorities are photon-engineered radiative cooling or thermally conductive fibers.[12,65] **Figure 3**a shows a 3D printed thermally conductive boron nitride (BN)/poly (vinyl alcohol) (PVA) composite fabric, in which BN nanosheets are uniformly dispersed and highly aligned. The highly oriented and interconnected BN nanosheets provide energetic pathways for phonon conduction to enhance heat dispersion. The manufactured a-BN/PVA fabric exhibits a high thermal conductivity. A wearable textile based on this fabric can effectively transfer the heat generated by the body from the skin to the cool surrounding environment, thereby bringing an attractive cooling effect to the human body.

In recent years, considering that human skin emits thermal radiation, photoengineered radiative cooling fibers with reasonably designed solar and mid-IR optical properties have also attracted considerable attention. Figure 3b displays the schematic diagram of the spectrally selective nanocomposite fabric for outdoor radiative cooling, in which zinc oxide nanoparticles (ZnO NPs) are embedded in nanoporous polyethylene (PE).[66] Like TPX, PE is transparent in the infrared spectrum, thus can effectively transmit out human body radiation. As a distinctive inorganic material, ZnO has a high refractive but little absorption from visible to mid-IR wavelengths. ZnO NPs with a particle size between 0.1 and 1 μm induce stronger Mie scattering in the visible range to achieve high reflection. The fibers are fabricated by melt extruding a paraffin oil solution of PE and ZnO, after which the paraffin oil is extracted to form nanopores. By calculating the optimized particle size and density, the obtained textile can prevent the simulated skin from overheating above 10 °C in an outdoor environment. Through similar extrusion and extraction approaches, Peng et al. manufactured a pure nanoporous PE fiber for radiative cooling, in which nanopores embedded in the fiber can directly scatter visible light (Figure 3c).[3] Compared with traditional textiles, nanoporous PE fabrics can reduce the temperature of human skin by 2.3 °C, thereby achieving considerable energy-saving effects. Subsequently, the researchers have also developed colored PE fibers by doping inorganic pigment particles without influencing the high infrared transparency. The colored PE fibers are also made by extrusion, and the knitted fabrics show good radiative cooling performance of 1.6 to 1.8 °C. This work provides hope for

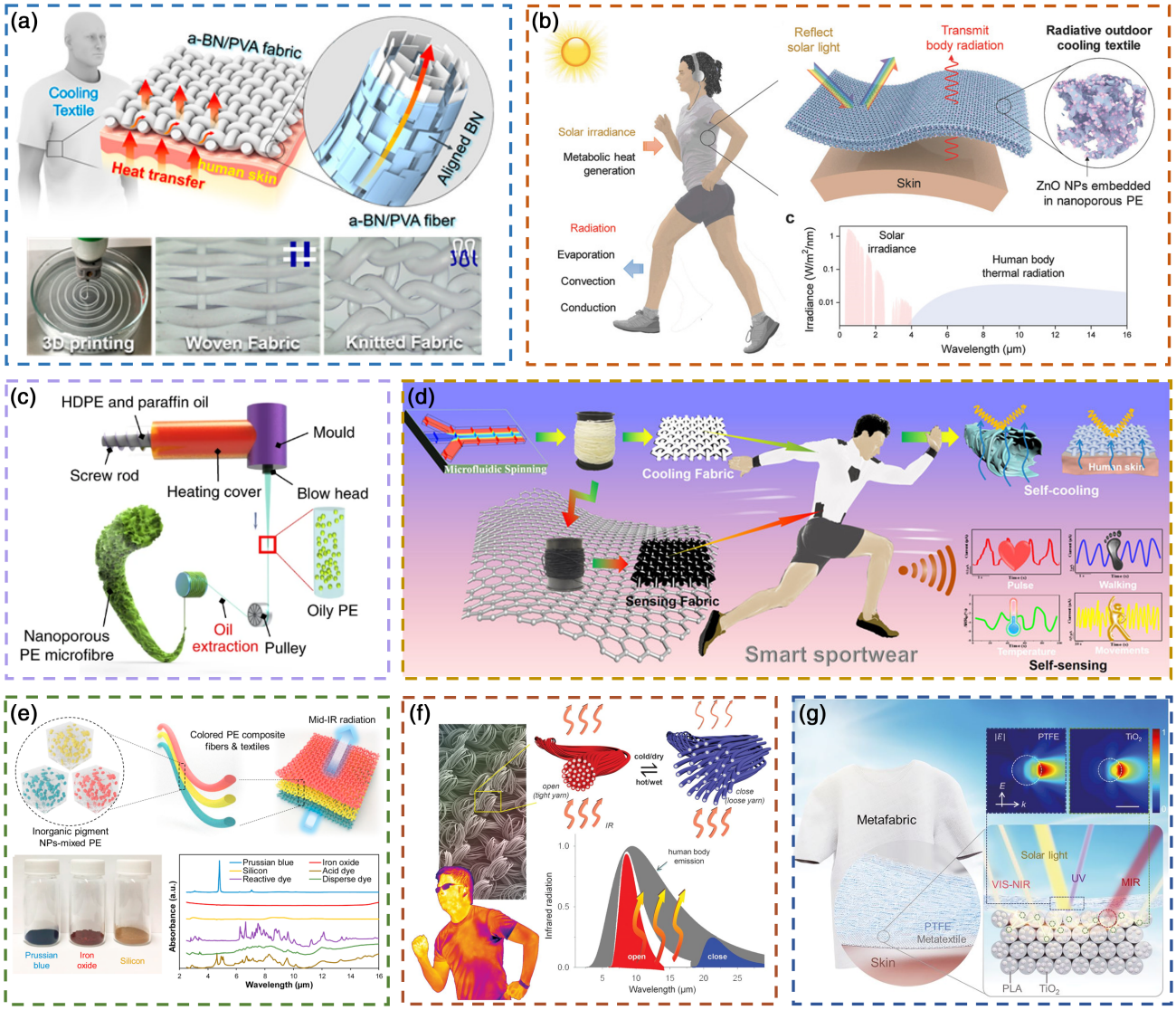

Figure 3. Various fibers used for human body cooling. a) Thermally conductive composite fabric. Reproduced with permission.[65] Copyright 2017, American Chemical Society. b) ZnO NPs embedded nanoporous PE fabric. Reproduced with permission.[66] Copyright 2018, Wiley-VCH GmbH. c) Nanoporous PE fiber. Reproduced with permission.[3] Copyright 2018, Springer Nature. d) Self-sensing and self-cooling integrated smart fiber. Reproduced with permission.[68] Copyright 2019, American Chemical Society. e) Colored PE fibers. Reproduced with permission.[67] Copyright 2019, Elsevier. f) Metafibers with self-adjustable infrared emissivity. Reproduced with permission.[33] Copyright 2019, AAAS. g) Hierarchical-morphology metafabric for scalable radiative cooling. Reproduced with permission.[69] Copyright 2021, AAAS.

the practical application and commercialization of radiative cooling textiles (Figure 3e).[67] Hu et al. further introduced self-cooling property into smart fibers.[68] As shown in Figure 3d, they fabricated a multiscale disordered porous polyurethane (PU) fiber with self-sensing and self-cooling capabilities. The fibers are manufactured by a microfluid spinning process and collected on a roller. Owing to the nonsolvent-induced phase separation, nano- and micropores are embedded into the PU skeletons. The pore sizes are in the visible wavelength range to scatter sunlight while reserving the infrared transparent property of PU. Real-time strain and temperature sensing functions are accomplished by decorating graphene nanosheets on the porous PU fibers and monitoring the resistance changes. Thus, a self-cooling fiber with personal thermal management capability is successfully constructed.

Different from the aforementioned infrared transparent fibers, Zhang et al. proposed a metafiber with self-adjustable emissivity in the atmospheric window (Figure 3f).[33] Hydrophobic triacetate and hydrophilic cellulose are adopted as base polymer materials to fabricate elliptically shaped bimorph fibers. The few-walled carbon nanotubes (CNTs) with tunable emissivity, excellent thermal conductivity, and good chemical stability are selected as meta-elements and coated on the bimorph fibers. As the humidity of the human skin changes, the triacetate

and cellulose components expand differentially due to hydrophobic and hydrophilic effects. When hot and/or wet, the cellulose can absorb water, causing the woven yarn to collapse and bringing CNTs closer together, triggering resonant electromagnetic coupling. The coupling increases the infrared emissivity of the fabric, thus enhancing the heat exchange. In contrast, when it is cold and/or dry, the infrared emissivity decreases, and the heat exchange reduces. Such temperature- and/or humidity-responsive metafibers are expected to be used in autonomous thermal management systems. Recently, Zeng et al. designed a multilayer metafabric with high emissivity in the atmospheric window, breaking through the thickness restrictions of mid-IR-transparent radiative cooling textiles reported previously.[69] The metafabric is fabricated by laminating a 50 μm-thick commercially available PTFE film with a TiO_2-PLA composite woven textile. TiO_2 nanoparticles are mixed with PLA in an optimized volume ratio by a twin-screw extruder, then the composite material is spun and finally drafted on a draw winder machine to obtain the metafibers. The doped TiO_2 nanoparticles possess a size between 200 and 1600 nm, producing high reflectivity in the Vis–NIR band through the collective effect of multiple Mie resonances. PLA is selected because of its abundant chemical bonds with rich emittance in the MIR waveband, high solar transmittance, hygroscopicity, and biodegradability. In practical application, the mass-produced metafabric with high emissivity in the atmospheric window can cool the covered human body by about 4.8 °C.

5. Fabrication of Metafibers by Thermal Drawing Technique

Compared with film structures, the woven structures in textiles exhibit the merits of air permeability, stretchability, better mechanical strength, and wearing comfort. Moreover, the woven textiles can easily accommodate complex deformations, enabling them to be applied in a variety of scenarios. As displayed in Figure 3, numerous efforts have been put into manufacturing radiative cooling fibers, such as 3D printing, extrusion, and spinning. However, these approaches either require tremendous time consumption or can only build simple structures, which are difficult to mass-produce fibers with complex structures. In addition, majorities of the radiative cooling textiles are IR transparent, so their thickness needs to be controlled to avoid decreasing the transparency, which will inevitably damage the mechanical strength and durability. Metafibers that exhibit high emissivity in the atmospheric window have only been proposed recently. These metafibers are not subject to strict thickness restrictions, thus facilitating their applications in real life. However, the construction of these metafibers relies on modification of commercially available fabrics, or multistep melt extrusion mixing, melt spinning and drafting processes, which are obviously limited in material selection and meta-element structure control. Finally, the current metafabrics are commonly fabricated by randomly mixing meta-elements, and the periodic structures with engineered dispersion diagrams in metafibers still need to be explored.[70,71]

Preform-to-fiber thermal drawing technique is expected to be a promising solution.[35,72–74] The thermal drawing technique was originally used in the fabrication of optical fibers, and has now been widely applied in various fields such as fiber-optic sensors, flexible electronics, and micro/nanofabrication.[75] In the thermal drawing process, a macroscopic preform is fed into a fiber drawing tower, heated to a viscous state at an elevated temperature, and necked under the action of gravity or an external force. The preform is then drawn into a kilometer-long microstructure fiber by applied tension while reserving its geometry and decreasing the cross-sectional dimension. The diameter of the obtained fiber can be easily controlled by adjusting the preform feed down speed and the fiber drawing speed. Therefore, the sophisticated structures in the microscopic fibers can be inherited from the macroscopic preforms, which greatly reduces the operation difficulty. Moreover, the thermal drawing technique is applicable to various materials, such as polymers, metals, semiconductors, and even liquids. With reasonable preform design, mass production of multimaterial and multifunctional fibers can be achieved. What is more fascinating is that recently, many post-treatment processes such as thermal processing,[37–42,45,76–79] cold drawing,[46] and imprinting,[48] have been applied to the fabricated fibers to construct various micro–nano structures. Compared with other metafiber manufacturing methods, the thermal drawing technique can break the material restrictions and introduce various meta-elements instead of just mixing with commercially available nanomaterials. The fabrication process is convenient and will not introduce unexpected reagents. The sizes of in-fiber particles and fiber surface structures range from nanoscale to microscale, and the morphologies and distributions are adjustable. Owing to the recent advancement of the Plateau-Rayleigh capillary (PR) instability in thermal treatment, mechanical-geometric mismatch in cold drawing, and surface imprinting process, periodic structures can be simply obtained, which is more conductive to achieve near-ideal strictly selective unity infrared emission and high solar reflection. These periodic structures are difficult to reach using other methods, such as mixing or spin coating. Moreover, the synergy of fiber surface patterns and in-fiber structures is expected to provide more superior spectral selectivity. Finally, the thermal drawing technique can integrate various functions in radiative cooling metafibers, such as physical sensing, chemical sensing, and energy management. This opens new opportunities to achieve smart metafabrics for sustainable radiative cooling.[52,80] In this section, the preparation of metafibers by the thermal drawing technique will be introduced in detail.

5.1. In-Fiber Structured Particles Generated by Thermal Processing

Figure 4 displays various in-fiber structured particles generated by fiber thermal treatments. PR capillary instability that minimizes surface energy lays the foundation of these results.[34,81] As shown in Figure 4a, Kaufman et al. fabricated a series of uniform and structured spherical particles by thermal processing of multimaterial fibers.[41] First, a core/cladding As_2Se_3/polyethersulphone (PES) preform is prepared and thermally drawn into a fiber with the desired core diameter. Then, the fiber undergoes thermal treatment, during which the viscosity of As_2Se_3 decreases. Owing to PR capillary instability, the continuous

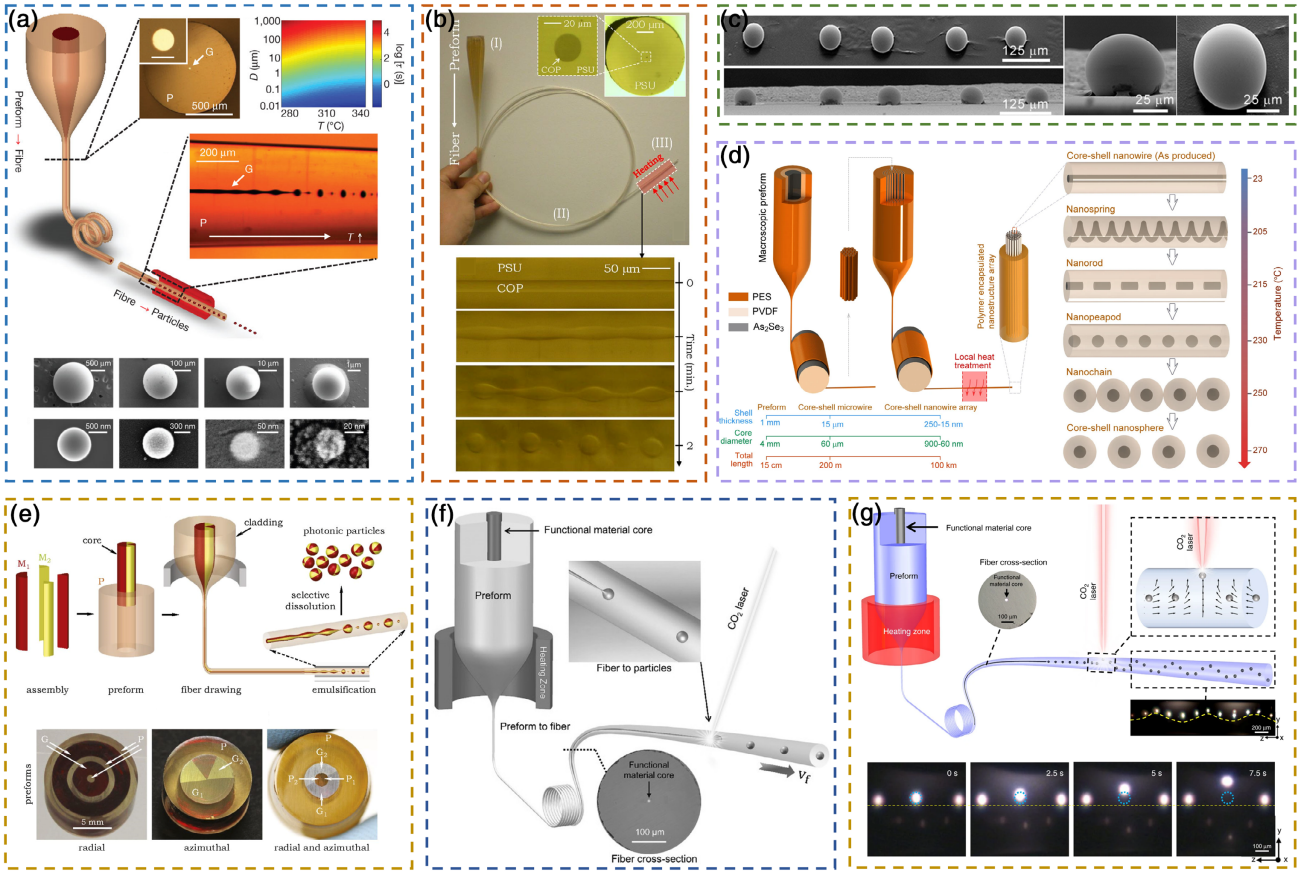

Figure 4. Various in-fiber structured particles generated by capillary instability induced by thermal processing. a) Structured spheres generated in glass-polymer fibers. Reproduced with permission.[41] Copyright 2012, Springer Nature. b) In-fiber production of polymeric particles. Reproduced with permission.[42] Copyright 2013, United States National Academy of Sciences. c) SEM images of an ellipsoid array and a single microellipsoid. Reproduced with permission.[45] Copyright 2014, Wiley-VCH GmbH. d) Tailoring self-organized nanostructured morphologies in fiber. Reproduced with permission.[40] Copyright 2014, Nature Research. e) Multimaterial photonic particles with controllable internal geometry. Reproduced with permission.[38] Copyright 2016, United States National Academy of Sciences. f) Laser-induced in-fiber spherical particles. Reproduced with permission.[78] Copyright 2017, Wiley-VCH GmbH. g) Manipulation of in-fiber particle migration. Reproduced with permission.[79] Copyright 2019, Springer Nature.

As_2Se_3 core breaks up into an orderly arrangement of spherical particles driven by the surface tension. The diameters of the obtained spherical particles are related to the fiber core diameters, spanning a wide range from 20 to 2 mm. Moreover, the inherent advantages of the thermal drawing technique endow this method with scalability. For example, by introducing multiple cores in the preform, the orderly distribution of particles in 3D space can be achieved. Core–shell, Janus, or even "beach ball" particles can be constructed through a more delicate preform design. This provides a novel approach for the large-scale fabrication of metafibers, in which the size, distribution, and material of the meta-elements can be designed. Subsequently, the researchers further used this method to construct polymeric micro- and nanoparticles in the fiber (Figure 4b).[42] Numerous optical, magnetic, and potentially plasmonic functionalities can be integrated into the polymeric particles by impregnating the fiber core with appropriate dopants during the preparation of preforms.

Aktas et al. applied mechanical deformation to the As_2Se_3/PES fiber during the thermal treatment, transforming the array of spheres into an array of triaxial ellipsoids, or even "cigar-shaped" bodies.[45] Figure 4c displays the SEM images of an ellipsoidal As_2Se_3 array and a single microellipsoid obtained by abrasing one side of the PES cladding and transferring the fiber to a substrate, and then dissolving the PES. In this way, the structures of engineered particles produced by thermal processing are expanded. Khudiyev et al. further demonstrated the more complex in-fiber nanostructures by exploring the transitory region during thermal processing.[40] As shown in Figure 4d, the As_2Se_3/PVDF nanowires are constructed using a multistep iterative thermal drawing process. In short, the As_2Se_3/PVDF/PES preform is first thermally drawn into microfibers with a diameter of 400 μm. Then a self-organized hexagonal array of 360 microfibers is inserted into a PES sheath and redrawn. The produced As_2Se_3/PVDF nanowires are encapsulated in a PES cladding and subjected to heat treatment. Owing to the thermal compatibility of the three materials, the gradual increase in temperature leads to the progressive transformation of nanowires into nanosprings, nanorods, nanopeapods, nanochains, until core–shell nanospheres. The process can be stopped at any point to preserve

the nanostructures. Hence, infinitely long in-fiber arrays with tailored, self-organized nanostructured morphologies can be fabricated, opening up whole new research fields. In addition to the tailoring of morphologies of the particles, Tao et al. reported the control of the internal geometry of spherical multimaterial photonic particles.[38] As shown in Figure 4e, several prefabricated segments of different materials are inserted into a cladding to manufacture the preform. After thermal drawing, the obtained fiber is heated to construct an array of photonic particles. The optical scattering characteristics of these prepared photonic particles can be tailored by simply changing the macroscopic preform to produce diverse internal nanoscale geometry. Figure 4e displays the cross-sections of three preforms with radial, azimuthal, and combined geometries. In principle, this method can produce spherical particles with arbitrary internal structure, enabling the digital design of photonic particles, thereby introducing new optical characteristics that are currently inaccessible by other approaches.

Recently, CO_2 laser with small beam size and precisely tunable power has been adopted to produce in-fiber spherical particles.[78] As depicted in Figure 4f, the core/cladding preform is thermally drawn into a multimaterial fiber, and then laser heating leads the core to break up into a chain of spheres. Researchers studied the influence of feed-in velocity on the breakup periods and sphere sizes of various materials in detail, and the diameters of the obtained spheres range from 200 nm to 250 μm. Compared with traditional isothermal heating methods (such as furnace or flame), CO_2 laser offers a small confined heating area, to avoid the generation of undesired satellite spheres (Figure 4a,b,e) and efficiently reduces core-to-sphere amplification ratio. Furthermore, the manipulation of in-fiber particle migration is realized via CO_2 laser-induced thermocapillary convection (Figure 4g).[79] The illustration in the upper right corner depicts the velocity distributions of the convection flows dragging the particles when heated by a CO_2 laser. The bottom shows how an in-fiber single particle migrates over time. The particle is dragged away from the fiber center and migrates toward the cladding surface where the laser is focused on. This phenomenon can be explained as the laser heating induced thermal liquefaction, which transforms the solid fiber cladding to an ideal fluidic media and enables in-fiber particles to relocate. This programmable laser heating process can precisely control the particle migrations to reconstruct the in-fiber components, making it possible to form a 3D complex functional structure in fibers.

5.2. In-Fiber Structured Fragmentation Generated by Cold Drawing

Shabahang et al. performed cold drawing in a thermally drawn multimaterial fiber with a brittle core and a ductile polymer cladding, resulting in a controllable and sequential fragmentation of the core along with the fiber.[46] As shown in **Figure 5**a, when axial stress is applied, necking occurs on the ductile polymer and expands uniformly throughout the sample length via propagation of the shoulder. Meanwhile, due to the mechanical–geometric mismatch between the core and the cladding, the brittle core fractures into an array of cylindrical rods in an orderly sequence. The average length of the cylindrical rods depends on the core diameter and Young's modulus of the core and cladding. This approach is also applicable to other fiber geometries, such as rectangular and equilaterally triangular. The researchers explored various complex in-fiber multicomponent nano- and microstructures with arbitrary cross-sectional geometries via cold drawing of multimaterial fibers. Although this method can mass produce a variety of perfect in-fiber array structures, there is only a few further research, especially the application of the obtained structures in the fields of optics, electricity, and so on.[82,83] Chen et al. sandwiched atomically thin transition metal dichalcogenides (TMDs)[84] and monolayer polycrystalline graphene (MPG)[85] between thermoplastic polymers, and achieved ordered and atomically perfect TMD nanoribbons and MPG ribbons by drawing, respectively (Figure 5b,c).

5.3. Ordered Surface Structured Fibers

Beyond the in-fiber structures constructed through postheating or cold-drawing processes, surface textured fibers have also been widely explored recently.[75] Usually, these structures are introduced into the macroscopic preforms by machining, laser etching, or soft lithography, and then scaled down after thermal drawing to make the microstructures remain in the obtained fibers. Yildirim et al. fabricated a star-shaped polyetherimide (PEI) fiber with ordered microgrooves on the fiber surface (**Figure 6**a).[47] Khudiyev et al. adopted a similar approach to achieve fiber surface gratings with periods down to about 600 nm on a rectangular cross-section (Figure 6b).[51] The patterned polycarbonate (PC) fiber surface behaves as an optical diffraction grating with the feature size equivalent to the visible light wavelengths. Hence, when viewed from different angles, the fibers show different colors, inducing large-scale, angle-dependent structural coloration in the woven textiles. The surface-patterned fibers present vast opportunities in plasmonic metasurfaces.

The complex textures within hollow channels of polymer fibers have also been demonstrated.[49] As shown in the lower part of Figure 4d, by codrawing two textured polymers (PC and sacrificial material carbon-black loaded polyethylene [cPE]) in intimate contact, the interfacial tension is reduced to avoid the structure collapse of smaller dimensions. The cPE part can be peeled off by a straightforward mechanical method to produce two textured PC ribbons. Compared with the directly constructed surface pattern (the upper part of Figure 4d), the SEM images show that the textures of the codrawn fibers are perfectly scaled down. Similarly, a sub-100 nm textured cylindrical fiber has been achieved by a three-step iterative thermal drawing process of a PC/poly(methyl methacrylate) interface (Figure 6c).[50]

However, the textured fibers obtained directly from thermally drawn specially designed preforms only have 1D micro/nanogrooves longitudinally due to structure elongation and polymer reflow, which restricts the development and applications of surface patterned fibers. Wang et al. proposed a direct imprinting thermal drawing (DITD) technique to prepare 2D micro/nanostructures on the fiber surface.[48] As depicted in Figure 6e, the unpatterned preform is fed into the fiber drawing tower to be heated and softened. After being stretched into a fiber, a pair of patterned rollers are fixed directly below the neck-down region.

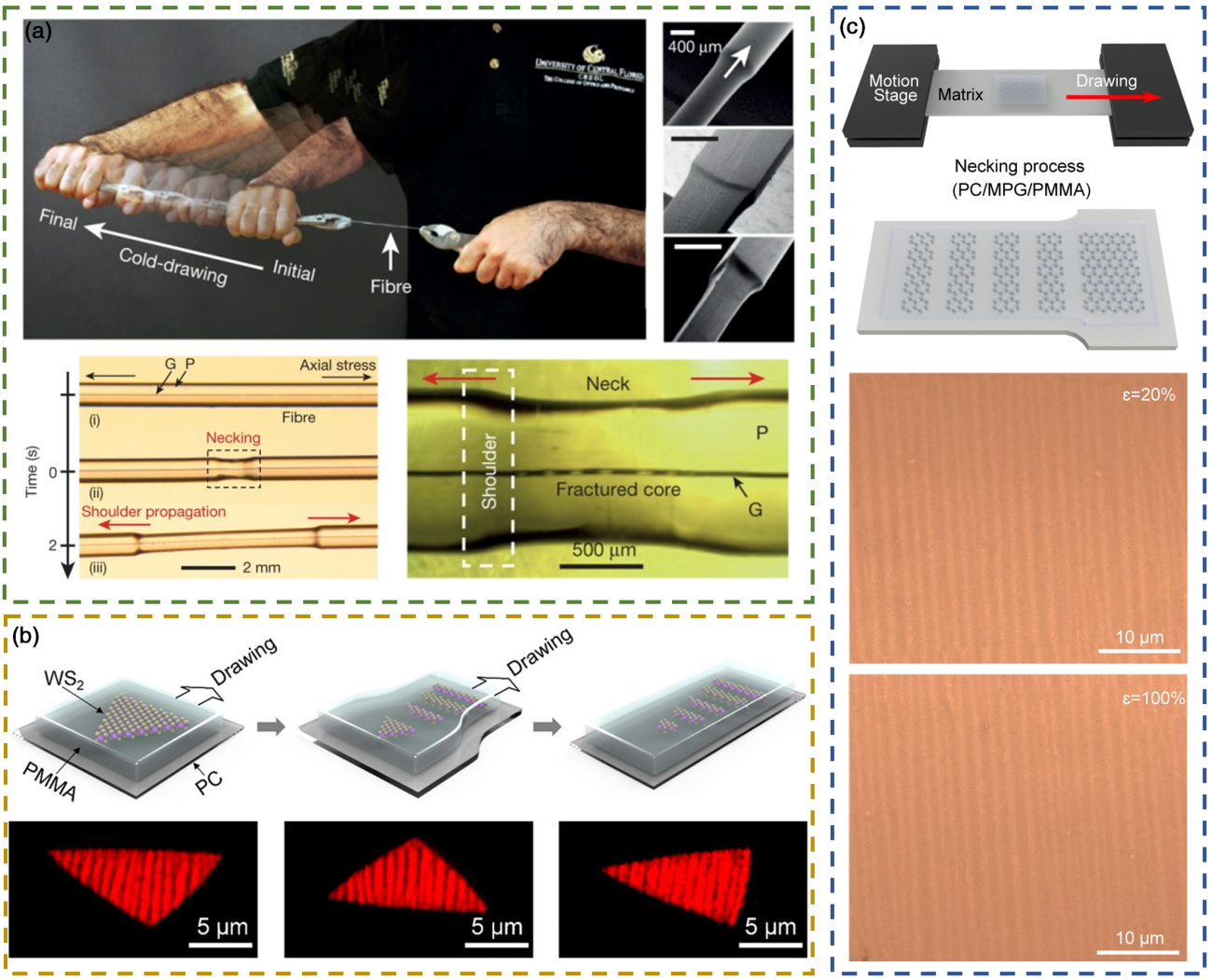

Figure 5. Various ordered structures generated by cold drawing. a) Controlled fragmentation of multimaterial fibers via cold drawing. Reproduced with permission.[46] Copyright 2016, Springer Nature. b) Ordered fragmentation of layered TMD. Reproduced with permission.[84] Copyright 2017, American Chemical Society. c) Controlled fragmentation of MPG. Reproduced with permission.[85] Copyright 2020, Elsevier.

As the fiber is still in a softened state, surface patterns can be produced on both sides of the fiber after being squeezed by the rollers. As the roller continues to rotate, the patterns are imprinted on the entire length of the fiber. The SEM image shows a 2D microdot array on the fiber surface, which behaves as a 2D diffraction grating under the irradiation of a white supercontinuum laser. After collecting the patterned fibers on a bobbin, the diffraction pattern can be observed. The DITD technique is applicable to various fiber materials, and numerous fiber surface patterns can be manufactured by directly changing the roller surface. The patterned feature size can be scaled down to tens of nanometers, showing great potential in plasmonic metasurfaces.

Moreover, fibers with other unique structures can also be manufactured by thermal drawing technique, such as fibers with well-ordered continuous nanowires,[86,87] fibers with spatially-selective porous domains,[88] fibers with aligned carbon nanofibers.[89] These structures have bright prospects in constructing metafibers for radiative cooling.[90] Although thermally drawn metafibers have not been used in the field of radiative cooling, it is believed that they possess great potential and will be vigorously developed in the future.

6. Conclusion

Radiative cooling harvesting the coldness from the universe without consuming external energy has great potential to alleviate global energy consumption and environmental pollution. Numerous metamaterials with subwavelength structures can be engineered to strongly couple to the incident electromagnetic waves and have been exploited for radiative cooling. However, complicated and delicate inorganic metamaterial structures fabricated by precision lithography or deposition require tremendous time and cost, and mass production is limited. A glass–polymer hybrid metamaterial film has only recently been

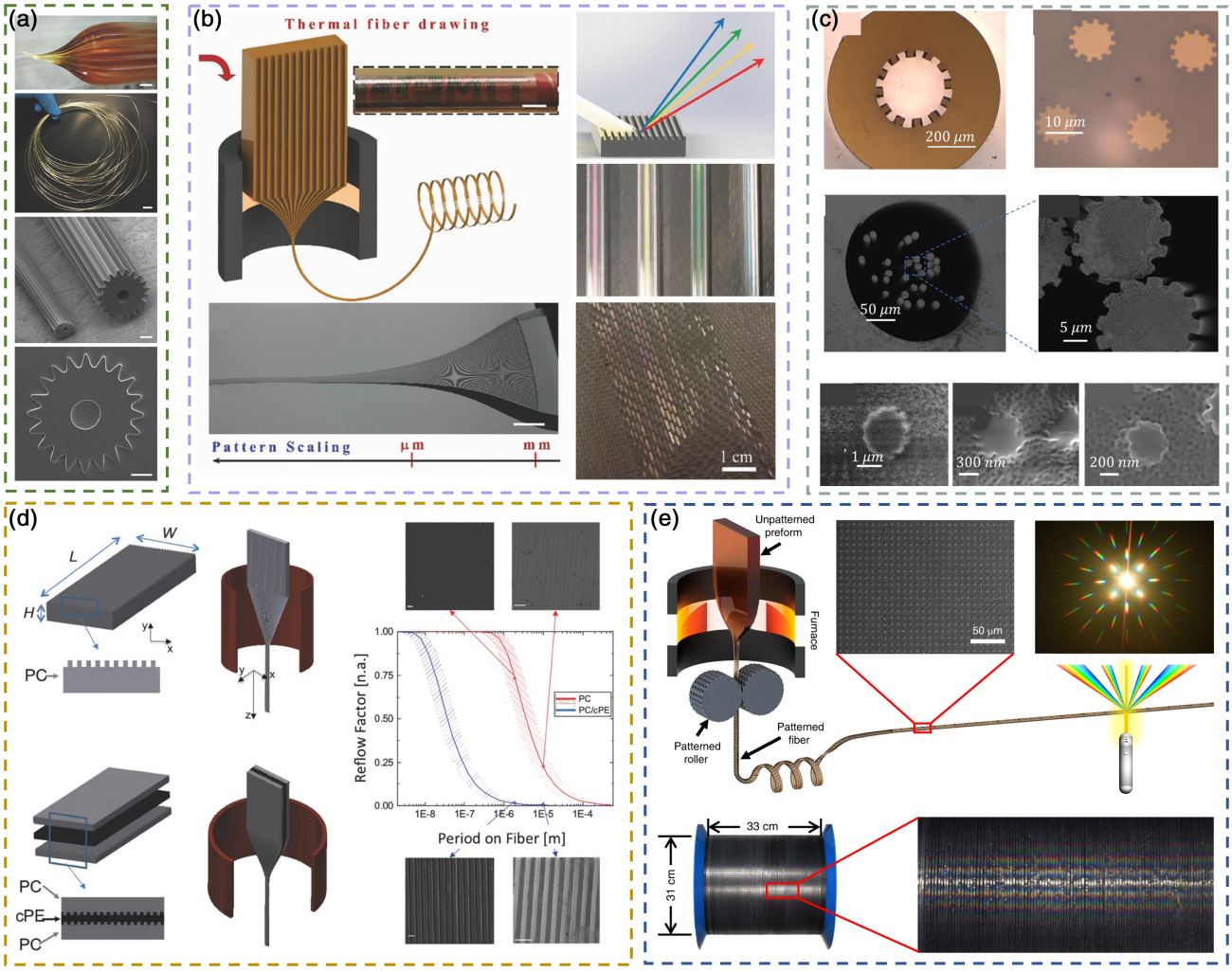

Figure 6. Ordered surface structure fibers manufactured by thermal drawing technique. a) ordered grooves on the microfibers. Reproduced with permission.[47] Copyright 2014, Wiley-VCH GmbH. b) Surface-patterned fibers for a diffraction grating. Reproduced with permission.[51] Copyright 2017, Wiley-VCH GmbH. c) Sub-100 nm textured fiber by PC/PMMA interface. Reproduced with permission.[50] Copyright 2019, American Institute of Physics. d) Sub-micrometer hierarchical textures by PC/cPE interface. Reproduced with permission.[49] Copyright 2017, Wiley-VCH GmbH. e) 2D micro/nanostructures on fiber surface generated by direct imprinting in thermal drawing (DITD). Reproduced with permission.[48] Copyright 2020, Springer Nature.

proposed, allowing radiative cooling materials with mass production capability and flexibility.

Flexible metamaterial can adhere to all surfaces in a conformal manner which ensures the bond of functional devices onto nonplanar surfaces. Additionally, the rendering flexibility of metamaterials allows lightweight and transparent metamaterials to surround objects. Metamaterial devices built on flexible and elastomeric substrates typically can be bent, stretched, and rolled, adding a new dimension to the manipulation of electromagnetic waves and guiding the design of metamaterial-based functional devices. However, large-area quasi-uniform flexible metamaterial is hard to achieve by standard top-down nanofabrication techniques, which is subject to complicated procedures and unevenly distributed fabrication.[91] Moreover, the absence of credible tuning techniques hampers the wide applications of these metamaterials. Tunability can be achieved to improve the device functionality by manipulating the interactions between the incident light and the metamaterials.

In addition, compared with films, textiles woven from fibers are air permeable, stretchable, and easy to accommodate complex deformations. Moreover, cooling the human body instead of the whole building can effectively reduce energy consumption. Although radiative cooling textiles have captured intensive research attention, majorities are IR transparent and have thickness restrictions. Metafibers with high emissivity in the atmospheric window have only recently been reported. In addition, radiative cooling fibers are usually fabricated by 3D printing, extrusion, or spinning, which limits the mass production of fibers with delicate structures. Appropriately ameliorated preform-to-fiber thermal drawing technique has great potential in solving this problem and realizing the large-scale production of quasi-uniform metamaterials with ultrawideband and tunable

spectrum response.[92,93] Thermal drawing technique starts from a macroscopic preform preparation, and the geometry of the preform is well preserved in the fabricated fiber. At the same time, thermal drawing technique applies to a variety of materials, including polymers, metals, semiconductors, and even liquids. Furthermore, the thermal drawing technique can produce nanoscale dimensions that would be difficult to manufacture by traditional methods.

In recent years, various postprocessing methods have been used to build micro- and nanostructures on the light wavelength scale in the resulting fibers or on the fiber surface. The first method exploits the PR capillary instability to generate various in-fiber structures by thermal treatment of multimaterial fibers. Through multicore design, in addition to spherical particles, core–shell, Janus, and even "beach ball" particles can be constructed. With reasonable temperature adjustment, the morphologies of the structures range from nanosprings, nanorods, nanopeapods, nanochains to nanospheres. Beyond glass materials, many in-fiber polymeric particles can also be produced, which are easily doped with optical, electrical, and magnetic properties. The particle size obtained from thermal treatment ranges from nanometers to millimeters, presenting a 1D to 3D distribution, meeting the requirements for constructing radiative cooling metamaterials. It is worth mentioning that the migration of the in-fiber particles can be accurately manipulated, which can enrich the family of multifunctional metafibers and achieve tunable optical properties. The second approach to postprocessing thermally drawn fibers is cold drawing, which breaks the brittle core in a ductile polymer cladding into an aligned array of microstructures. This surprising phenomenon makes it possible to construct metafibers in an extremely simple and straightforward manner. The third method is to pattern the fiber surface by patterned preform or roller embossing. The micro and nanoscale textures on the fiber surface can be used to control the optical properties, making them suitable for diffraction gratings and plasmonic metasurfaces. The synergy of fiber surface patterns and in-fiber structures can create more advanced functionalities, paving the way to constructing spectrally selective metafibers.

The time-saving and easy-fabricated thermal drawing technique, therefore, provides a powerful platform for future large-scale production of high-performance flexible metamaterial devices. The thermal drawing technique can also impart different colors to fibers through microstructures, impart health monitoring functions to wearable fabrics through stretchable materials, and even be used in biological platforms, etc.[94–96] These functions are expected to be combined with radiative cooling metafibers to realize multifunctional wearable fabrics. Hence, applying the thermal drawing technique to manufacture metafibers for radiative cooling has bright prospects, which is expected to inspire the development of a new generation of smart fabrics to reduce energy consumption and improve human life.

Acknowledgements

M.Q. and T.W. contributed equally to this work. This work was supported by the Singapore Ministry of Education Academic Research Fund Tier 2 (MOE2019-T2-2-127 and MOE-T2EP50120-0002), A*STAR under AME IRG (A2083c0062), the Singapore Ministry of Education Academic Research Fund Tier 1 (RG90/19 and RG73/19) and the Singapore National Research Foundation Competitive Research Program (NRF-CRP18-2017-02). This study was supported under the RIE2020 Industry Alignment Fund - Industry Collaboration Projects (IAF-ICP) Funding Initiative I2001E0067 (IAF-ICP) - P2.1, as well as cash and in-kind contribution from Schaeffler (Singapore) Pte Ltd. This work was also supported by Nanyang Technological University.

Conflict of Interest

The authors declare no conflict of interest.

Keywords

metafibers, metamaterials, radiative cooling, thermal drawing techniques

Received: October 7, 2021
Revised: October 24, 2021
Published online: November 16, 2021

[1] A. S. Farooq, P. Zhang, *Composites, Part A* **2020**, *142*, 106249.
[2] A. M. Omer, *Renewable Sustainable Energy Rev.* **2008**, *12*, 2265.
[3] Y. Peng, J. Chen, A. Y. Song, P. B. Catrysse, P. Hsu, L. Cai, B. Liu, Y. Zhu, G. Zhou, D. S. Wu, H. R. Lee, S. Fan, Y. Cui, *Nat. Sustainability* **2018**, *1*, 105.
[4] Z. Ma, D. Zhao, C. She, Y. Yang, R. Yang, *Mater. Today Phys.* **2021**, *20*, 100465.
[5] E. Pakdel, M. Naebe, L. Sun, X. Wang, *ACS Appl. Mater. Interfaces* **2019**, *11*, 13039.
[6] X. Sun, Y. Sun, Z. Zhou, M. A. Alam, P. Bermel, *Nanophotonics* **2017**, *6*, 997.
[7] X. Yin, R. Yang, G. Tan, S. Fan, *Science* **2020**, *370*, 786.
[8] P. C. Hsu, A. Y. Song, P. B. Catrysse, C. Liu, Y. Peng, J. Xie, S. Fan, Y. Cui, *Science* **2016**, *353*, 1019.
[9] S. H. Choi, S. W. Kim, Z. Ku, M. A. Visbal-Onufrak, S. R. Kim, K. H. Choi, H. Ko, W. Choi, A. M. Urbas, T. W. Goo, Y. L. Kim, *Nat. Commun.* **2018**, *9*, 1.
[10] J. W. Leem, M. J. Fraser, Y. L. Kim, *Annu. Rev. Biomed. Eng.* **2020**, *22*, 79.
[11] J. W. Leem, A. E. L. Allcca, Y. J. Kim, J. Park, S. W. Kim, S. R. Kim, W. H. Ryu, Y. P. Chen, Y. L. Kim, *Adv. Biosyst.* **2020**, *4*, 2000040.
[12] P. C. Hsu, X. Li, *Science* **2020**, *370*, 784.
[13] D. Zhao, A. Aili, Y. Zhai, S. Xu, G. Tan, X. Yin, R. Yang, *Appl. Phys. Rev.* **2019**, *6*, 021306.
[14] J. P. Bijarniya, J. Sarkar, P. Maiti, *Renewable Sustainable Energy Rev.* **2020**, *133*, 110263.
[15] M. Zeyghami, D. Y. Goswami, E. Stefanakos, *Sol. Energy Mater. Sol. Cells* **2018**, *178*, 115.
[16] M. Santamouris, J. Feng, *Buildings* **2018**, *8*, 168.
[17] E. Rephaeli, A. Raman, S. Fan, *Nano Lett.* **2013**, *13*, 1457.
[18] L. Zhu, A. Raman, S. Fan, *Appl. Phys. Lett.* **2013**, *103*, 223902.
[19] L. Zhu, A. Raman, K. X. Wang, M. A. Anoma, S. Fan, *Optica* **2014**, *1*, 32.
[20] L. Zhu, A. P. Raman, S. Fan, *PNAS* **2015**, *112*, 12282.
[21] A. P. Raman, M. A. Anoma, L. Zhu, E. Rephaeli, S. Fan, *Nature* **2014**, *515*, 540.
[22] Z. Chen, L. Zhu, A. Raman, S. Fan, *Nat. Commun.* **2016**, *7*, 1.
[23] M. Ono, K. Chen, W. Li, S. Fan, *Opt. Express* **2018**, *26*, A777.
[24] D. Wu, C. Liu, Z. Xu, Y. Liu, Z. Yu, L. Yu, L. Chen, R. Li, R. Ma, H. Ye, *Mater. Des.* **2018**, *139*, 104.
[25] M. M. Hossain, B. Jia, M. Gu, *Adv. Opt. Mater.* **2015**, *3*, 1047.

[26] Y. Zhai, Y. Ma, S. N. David, D. Zhao, R. Lou, G. Tan, R. Yang, X. Yin, *Science* **2017**, *355*, 1062.
[27] C. Zou, G. Ren, M. M. Hossain, S. Nirantar, W. Withayachumnankul, T. Ahmed, M. Bhaskaran, S. Sriram, M. Gu, C. Fumeaux, *Adv. Opt. Mater.* **2017**, *5*, 1700460.
[28] D. Zhao, A. Aili, Y. Zhai, J. Lu, D. Kidd, G. Tan, X. Yin, R. Yang, *Joule* **2019**, *3*, 111.
[29] S. Y. Heo, G. J. Lee, D. H. Kim, Y. J. Kim, S. Ishii, M. S. Kim, T. J. Seok, B. J. Lee, H. Lee, Y. M. Song, *Sci. Adv.* **2020**, *6*, eabb1906.
[30] J. Song, J. Seo, J. Han, J. Lee, B. J. Lee, *Appl. Phys. Lett.* **2020**, *117*, 094101.
[31] Y. N. Liu, X. L. Weng, P. Zhang, W. X. Li, Y. Gong, L. Zhang, T. C. Han, P. H. Zhou, L. J. Deng, *Chinese Phys. Lett.* **2021**, *38*, 034201.
[32] B. Ko, D. Lee, T. Badloe, J. Rho, *Energies* **2019**, *12*, 89.
[33] X. A. Zhang, S. Yu, B. Xu, M. Li, Z. Peng, Y. Wang, S. Deng, X. Wu, Z. Wu, M. Ouyang, Y. Wang, *Science* **2019**, *363*, 619.
[34] B. Xu, S. Ma, Y. Xiang, J. Zhang, M. Zhu, L. Wei, G. Tao, D. Deng, *Adv. Fiber Mater.* **2020**, *2*, 1.
[35] G. Loke, W. Yan, T. Khudiyev, G. Noel, Y. Fink, *Adv. Mater.* **2020**, *32*, 1904911.
[36] W. Yan, C. Dong, Y. Xiang, S. Jiang, A. Leber, G. Loke, W. Xu, C. Hou, S. Zhou, M. Chen, R. Hu, P. P. Shum, L. Wei, X. Jia, F. Sorin, X. Tao, G. Tao, *Mater. Today* **2020**, *35*, 168.
[37] L. Wei, C. Hou, E. Levy, G. Lestoquoy, A. Gumennik, A. F. Abouraddy, J. D. Joannopoulos, Y. Fink, *Adv. Mater.* **2017**, *29*, 1603033.
[38] G. Tao, J. J. Kaufman, S. Shabahang, R. R. Naraghi, S. V. Sukhov, J. D. Joannopoulos, Y. Fink, A. Dogariu, A. F. Abouraddy, *PNAS* **2016**, *113*, 6839.
[39] T. C. Lin, J. Zhao, C. Cao, A. Javadi, Y. Yang, I. Hwang, X. Li, *J. Micro Nano-Manuf.* **2016**, *4*, 041008.
[40] T. Khudiyev, O. Tobail, M. Bayindir, *Sci. Rep.* **2014**, *4*, 1.
[41] J. J. Kaufman, G. Tao, S. Shabahang, E. H. Banaei, D. S. Deng, X. Liang, S. G. Johnson, Y. Fink, A. F. Abouraddy, *Nature* **2012**, *487*, 463.
[42] J. J. Kaufman, R. Ottman, G. Tao, S. Shabahang, E. H. Banaei, X. Liang, S. G. Johnson, Y. Fink, R. Chakrabarti, A. F. Abouraddy, *PNAS* **2013**, *110*, 15549.
[43] D. S. Deng, N. D. Orf, A. F. Abouraddy, A. M. Stolyarov, J. D. Joannopoulos, H. A. Stone, Y. Fink, *Nano Lett.* **2008**, *8*, 4265.
[44] D. S. Deng, J. C. Nave, X. Liang, S. G. Johnson, Y. Fink, *Opt. Express* **2011**, *19*, 16273.
[45] O. Aktas, E. Ozgur, O. Tobail, M. Kanik, E. Huseyinoglu, M. Bayindir, *Adv. Opt. Mater.* **2014**, *2*, 618.
[46] S. Shabahang, G. Tao, J. J. Kaufman, Y. Qiao, L. Wei, T. Bouchenot, A. P. Gordon, Y. Fink, Y. Bai, R. S. Hoy, A. F. Abouraddy, *Nature* **2016**, *534*, 529.
[47] A. Yildirim, M. Yunusa, F. E. Ozturk, M. Kanik, M. Bayindir, *Adv. Funct. Mater.* **2014**, *24*, 4569.
[48] Z. Wang, T. Wu, Z. Wang, T. Zhang, M. Chen, J. Zhang, L. Liu, M. Qi, Q. Zhang, J. Yang, W. Liu, H. Chen, Y. Luo, L. Wei, *Nat. Commun.* **2020**, *11*, 1.
[49] T. N. Dang, A. C. De Luca, W. Yan, Y. Qu, A. G. Page, M. Volpi, T. Das Gupta, S. P. Lacour, F. Sorin, *Adv. Funct. Mater.* **2017**, *27*, 1605935.
[50] T. N. Dang, I. Richard, E. Goy, F. Sordo, F. Sorin, *J. Appl. Phys.* **2019**, *125*, 175301.
[51] T. Khudiyev, C. Hou, A. M. Stolyarov, Y. Fink, *Adv. Mater.* **2017**, *29*, 1605868.
[52] S. Xue, G. W. Barton, S. Fleming, A. Argyros, *J. Light. Technol.* **2017**, *35*, 2167.
[53] O. Meangbua, S. Dhakal, J. K. M. Kuwornu, *Energy Policy* **2019**, *129*, 521.
[54] D. Chae, M. Kim, P. H. Jung, S. Son, J. Seo, Y. Liu, B. J. Lee, H. Lee, *ACS Appl. Mater. Interfaces* **2020**, *12*, 8073.
[55] S. Fan, A. Raman, *Natl. Sci. Rev.* **2018**, *5*, 132.
[56] M. A. Kecebas, M. P. Menguc, A. Kosar, K. Sendur, *J Quant Spectrosc Radiat Transf* **2017**, *198*, 179.
[57] J. Kou, Z. Jurado, Z. Chen, S. Fan, A. J. Minnich, *ACS Photonics* **2017**, *4*, 626.
[58] S. Taylor, Y. Yang, L. Wang, *J. Quant. Spectrosc. Radiat. Transfer* **2017**, *197*, 76.
[59] P. Yang, C. Chen, Z. M. Zhang, *Sol. Energy* **2018**, *169*, 316.
[60] T. Suichi, A. Ishikawa, Y. Hayashi, K. Tsuruta, *AIP Adv.* **2018**, *8*, 055124.
[61] S. Atiganyanun, J. B. Plumley, S. J. Han, K. Hsu, J. Cytrynbaum, T. L. Peng, S. M. Han, S. E. Han, *ACS Photonics* **2018**, *5*, 1181.
[62] J. Yang, X. Gao, Y. Wu, T. Zhang, H. Zeng, X. Li, *Sol. Energy Mater. Sol. Cells* **2020**, *206*, 110301.
[63] J. Feng, M. Santamouris, K. Gao, *Sol. Energy Mater. Sol. Cells* **2020**, *215*, 110671.
[64] L. Yang, H. Yan, J. C. Lam, *Appl. Energy* **2014**, *115*, 164.
[65] T. Gao, Z. Yang, C. Chen, Y. Li, K. Fu, J. Dai, E. M. Hitz, H. Xie, B. Liu, J. Song, B. Yang, L. Hu, *ACS Nano* **2017**, *11*, 11513.
[66] L. Cai, A. Y. Song, W. Li, P. C. Hsu, D. Lin, P. B. Catrysse, Y. Liu, Y. Peng, J. Chen, H. Wang, J. Xu, A. Yang, S. Fan, Y. Cui, *Adv. Mater.* **2018**, *30*, 1802152.
[67] L. Cai, Y. Peng, J. Xu, C. Zhou, C. Zhou, P. Wu, D. Lin, S. Fan, Y. Cui, *Joule* **2019**, *3*, 1478.
[68] X. Hu, M. Tian, T. Xu, X. Sun, B. Sun, C. Sun, X. Liu, X. Zhang, L. Qu, *ACS Nano* **2019**, *14*, 559.
[69] S. Zeng, S. Pian, M. Su, Z. Wang, M. Wu, X. Liu, M. Chen, Y. Xiang, J. Wu, M. Zhang, Q. Cen, Y. Tang, X. Zhou, Z. Huang, R. Wang, A. Tunuhe, X. Sun, Z. Xia, M. Tian, M. Chen, X. Ma, L. Yang, J. Zhou, H. Zhou, Q. Yang, X. Li, Y. Ma, G. Tao, *Science* **2021**, *373*, 692.
[70] A. Ahmadi, H. Mosallaei, *Phys. Rev. B* **2008**, *77*, 045104.
[71] S. J. Corbitt, M. Francoeur, B. Raeymaekers, *J. Quant. Spectrosc. Radiat. Transfer* **2015**, *158*, 3.
[72] Y. Qu, T. N. Dang, A. G. Page, W. Yan, T. D. Gupta, G. M. Rotaru, R. M. Rossi, V. D. Favrod, N. Bartolomei, F. Sorin, *Adv. Mater.* **2018**, *30*, 1707251.
[73] M. Chen, Z. Wang, K. Li, X. Wang, L. Wei, *Adv. Fiber Mater.* **2021**, *3*, 1.
[74] J. Zhang, Z. Wang, Z. Wang, L. Wei, *J. Light. Technol.* **2021**, *39*, 3836.
[75] Z. Wang, M. Chen, Y. Zheng, J. Zhang, Z. Wang, J. Yang, Q. Zhang, B. He, M. Qi, H. Zhang, K. Li, L. Wei, *Adv. Dev. Instrum.* **2021**, *2021*, 9676470.
[76] A. Gumennik, L. Wei, G. Lestoquoy, A. M. Stolyarov, X. Jia, P. H. Rekemeyer, M. J. Smith, X. Liang, B. J.-B. Grena, S. G. Johnson, S. Gradečak, A. F. Abouraddy, J. D. Joannopoulos, Y. Fink, *Nat. Commun.* **2013**, *4*, 1.
[77] A. Gumennik, E. C. Levy, B. Grena, C. Hou, M. Rein, A. F. Abouraddy, J. D. Joannopoulos, Y. Fink, *PNAS* **2017**, *114*, 7240.
[78] J. Zhang, K. Li, T. Zhang, P. J. S. Buenconsejo, M. Chen, Z. Wang, M. Zhang, Z. Wang, L. Wei, *Adv. Funct. Mater.* **2017**, *27*, 1703245.
[79] J. Zhang, Z. Wang, Z. Wang, T. Zhang, L. Wei, *Nat. Commun.* **2019**, *10*, 1.
[80] A. Tuniz, B. T. Kuhlmey, R. Lwin, A. Wang, J. Anthony, R. Leonhardt, S. C. Fleming, *Appl. Phys. Lett.* **2010**, *96*, 191101.
[81] S. Shabahang, J. J. Kaufman, D. S. Deng, A. F. Abouraddy, *Appl. Phys. Lett.* **2011**, *99*, 161909.
[82] K. Xu, Z. Wang, C. F. Tan, N. Kang, L. Chen, L. Ren, E. S. Thian, G. W. Ho, R. Ji, M. Hong, *ACS Appl. Mater. Interfaces* **2017**, *9*, 26341.
[83] K. Li, N. Zhang, T. Zhang, Z. Wang, M. Chen, T. Wu, S. Ma, M. Zhang, J. Zhang, D. U. S., P. P. Shum, M. Olivoc, L. Wei, *J. Mater. Chem. C* **2018**, *6*, 4649.

[84] M. Chen, J. Xia, J. Zhou, Q. Zeng, K. Li, K. Fujisawa, W. Fu, T. Zhang, J. Zhang, Z. Wang, Z. Wang, X. Jia, M. Terrones, Z. X. Shen, Z. Liu, L. Wei, *ACS Nano* **2017**, *11*, 9191.
[85] M. Chen, Z. Wang, X. Ge, Z. Wang, K. Fujisawa, J. Xia, Q. Zeng, K. Li, T. Zhang, Q. Zhang, M. Chen, N. Zhang, T. Wu, S. Ma, G. Gu, Z. Shen, L. Liu, Z. Liu, L. Wei, *Matter* **2020**, *2*, 666.
[86] M. Yaman, T. Khudiyev, E. Ozgur, M. Kanik, O. Aktas, E. O. Ozgur, H. Deniz, E. Korkut, M. Bayindir, *Nat. Mater.* **2011**, *10*, 494.
[87] J. J. Kaufman, G. Tao, S. Shabahang, D. S. Deng, Y. Fink, A. F. Abouraddy, *Nano Lett.* **2011**, *11*, 4768.
[88] B. Grena, J. B. Alayrac, E. Levy, A. M. Stolyarov, J. D. Joannopoulos, Y. Fink, *Nat. Commun.* **2017**, *8*, 1.
[89] Y. Guo, S. Jiang, B. J. B. Grena, I. F. Kimbrough, E. G. Thompson, Y. Fink, H. Sontheimer, T. Yoshinobu, X. Jia, *ACS Nano* **2017**, *11*, 6574.
[90] H. Zhong, Y. Li, P. Zhang, S. Gao, B. Liu, Y. Wang, T. Meng, Y. Zhou, H. Hou, C. Xue, Y. Zhao, Z. Wang, *ACS Nano* **2021**, *15*, 10076.
[91] T. Wu, K. Li, N. Zhang, J. Xia, Q. Zeng, X. Wen, U. S. Dinish, M. Olivo, Z. Shen, Z. Liu, Q. Xiong, Y. Luo, S. A. Maier, L. Wei, *Adv. Opt. Mater.* **2019**, *7*, 1900905.
[92] T. Zhang, K. Li, J. Zhang, M. Chen, Z. Wang, S. Ma, N. Zhang, L. Wei, *Nano Energy* **2017**, *41*, 35.
[93] A. F. Abouraddy, M. Bayindir, G. Benoit, S. D. Hart, K. Kuriki, N. Orf, O. Shapira, F. Sorin, B. Temelkuran, Y. Fink, *Nat. Mater.* **2007**, *6*, 336.
[94] T. Khudiyev, J. Clayton, E. Levy, N. Chocat, A. Gumennik, A. M. Stolyarov, J. Joannopoulos, Y. Fink, *Nat. Commun.* **2017**, *8*, 1.
[95] A. Leber, C. Dong, R. Chandran, T. D. Gupta, N. Bartolomei, F. Sorin, *Nat. Electron.* **2020**, *3*, 316.
[96] S. Park, Y. Guo, X. Jia, H. K. Choe, B. Grena, J. Kang, J. Park, C. Lu, A. Canales, R. Chen, Y. S. Yim, G. B. Choi, Y. Fink, P. Anikeeva, *Nat. Neurosic.* **2017**, *20*, 612.
[97] D. Li, X. Liu, W. Li, Z. Lin, B. Zhu, Z. Li, J. Li, B. Li, S. Fan, J. Xie, J. Zhu, *Nat. Nanotechnol.* **2021**, *16*, 153.
[98] Y. Xu, B. Sun, Y. Ling, Q. Fei, Z. Chen, X. Li, P. Guo, N. Jeon, S. Goswami, Y. Liao, S. Ding, Q. Yu, J. Lin, G. Huang, Z. Yan, *PNAS* **2020**, *117*, 205.
[99] A. Leroy, B. Bhatia, C. C. Kelsall, A. Castillejo-Cuberos, M. Di Capua H., L. Zhao, L. Zhang, A. M. Guzman, E. N. Wang, *Sci. Adv.* **2019**, *5*, eaat9480.
[100] A. Yang, L. Cai, R. Zhang, J. Wang, P. C. Hsu, H. Wang, G. Zhou, J. Xu, Y. Cui, *Nano Lett.* **2017**, *17*, 3506.
[101] J. Mandal, Y. Fu, A. C. Overvig, M. Jia, K. Sun, N. N. Shi, H. Zhou, X. Xiao, N. Yu, Y. Yang, *Science* **2018**, *362*, 315.
[102] P. C. Hsu, C. Liu, A. Y. Song, Z. Zhang, Y. Peng, J. Xie, K. Liu, C. L. Wu, P. B. Catrysse, L. Cai, S. Zhai, A. Majumdar, S. Fan, Y. Cui, *Sci. Adv.* **2017**, *3*, e1700895.
[103] R. Xiao, C. Hou, W. Yang, Y. Su, Y. Li, Q. Zhang, P. Gao, H. Wang, *ACS Appl. Mater. Interfaces* **2019**, *11*, 44673.

Lei Wei is an associate professor at Nanyang Technological University in Singapore. His main research interests are fiber-based devices, multifunctional fibers, bio-fiber interfaces, and in-fiber energy generation and storage. He serves as the Director of Centre for Optical Fibre Technology (COFT) at Nanyang Technological University. He also serves as the Chair of The Optical Society (OSA) Singapore Section and the Executive Committee Member of IEEE Photonics Society Singapore Chapter.